catalysts

MDPI

Article

Photocatalytic Degradation of Different VOCs in the Gas-Phase over TiO_2 Thin Films Prepared by Ultrasonic Spray Pyrolysis

Ibrahim Dundar [1,*], Marina Krichevskaya [2,*], Atanas Katerski [1], Malle Krunks [1] and Ilona Oja Acik [1,*]

1 Department of Materials and Environmental Technology, Laboratory of Thin Film Chemical Technologies Tallinn University of Technology, Ehitajate tee 5, 19086 Tallinn, Estonia; atanas.katerski@taltech.ee (A.K.); malle.krunks@taltech.ee (M.K.)

2 Department of Materials and Environmental Technology, Laboratory of Environmental Technology, Tallinn University of Technology, Ehitajate tee 5, 19086 Tallinn, Estonia

* Correspondence: ibrahim.dundar@taltech.ee (I.D.); marina.kritsevskaja@taltech.ee (M.K.); ilona.oja@taltech.ee (I.O.A.)

Received: 20 September 2019; Accepted: 31 October 2019; Published: 2 November 2019

Abstract: In this study, we deposited TiO_2 thin films onto borosilicate glass by ultrasonic spray pyrolysis at 350 and 450 °C. The aim of study is to determine the effect of deposition temperature on photocatalytic activity of TiO_2 thin films and to investigate the performance of TiO_2 thin films on photocatalytic degradation of methyl tert-butyl ether (MTBE), acetone, acetaldehyde, and heptane as functions of different operating parameters. TiO_2 thin films deposited at 350 and 450 °C have a thickness value of 190 and 330 nm, respectively. All as-prepared TiO_2 films possess an anatase crystalline structure. According to the X-ray photon spectroscopy (XPS) study, the TiO_2 thin film deposited at 350 °C showed a higher amount of oxygen vacancies and hydroxyl groups on the film surface after UV treatment. The aged-TiO_2 thin film deposited at 350 °C showed a water contact angle (WCA) value of 0° after 10 min UV irradiation, showing superhydrophilic surface behavior. The TiO_2 film deposited at 350 °C exhibited the highest amount of conversion of MTBE (100%). The results also showed that TiO_2 films are capable of photocatalytic degradation of MTBE (100%) and acetaldehyde (approx. 80%) in humid air conditions and high airflow rate. The visible-light-activity of TiO_2 thin films was tested with 5 ppm MTBE and acetone. TiO_2 thin films deposited at 350 °C with a surface area of 600 cm^2 showed 60% of MTBE and 33% of acetone degradation under VIS light.

Keywords: TiO_2; thin film; spray pyrolysis; photocatalytic; VOCs; indoor air; superhydrophilic

1. Introduction

Volatile organic compounds (VOCs) are the most common air pollutants, which are present in both indoor and outdoor air. It was reported that the VOC concentration indoors is often 2 to 5 times higher than that of the outdoors [1]. Among VOCs, acetone and acetaldehyde are common chemicals used extensively in a variety of industrial and domestic applications and are found in appreciable concentrations in indoor air [2,3]. Methyl tert-butyl ether (MTBE) and heptane are fuel components released to the atmosphere from gasoline and motor vehicle exhaust [4,5]. They are considered as outdoor generated VOCs, which also affect indoor air quality, especially in buildings close to parking lots or streets. Therefore, it is essential to obtain healthy living environments in modern buildings, integrated with air cleaning solutions [6]. According to the international standard, acetone and acetaldehyde together with heptane, toluene, and formaldehyde are the model air pollutants for the potential international standard testing of air cleaners [7].

The most widely studied semiconductor materials as photocatalysts in air treatment systems are commercial TiO_2 nanopowders such as P25, UV100, PC105, and PC500 and coatings prepared by those powders [8–11]. These are expected to have a high photocatalytic activity for gas-phase pollutant degradation due to their large available surface area. However, nanopowder coatings have high potential to agglomerate and detach from the substrate, causing a reduction in their photocatalytic activity [12,13] and low transmittance in the visible spectral range [14], which limits the field of applications such as indoor or outdoor photocatalysts.

Nanocrystalline TiO_2 thin films, however, are vital for safeguarding human health due to their strong adhesion to the substrate. Thus, the synthesis of thin films has advantages in the development of sustainable photocatalysts for applications containing flowing gas streams compared to nanopowder coatings [12,13]. The photocatalytic performance of TiO_2 thin films depends on several factors mostly related to thin film properties, primarily conditioned by the preparation method. Photocatalytic thin films can be fabricated by vacuum and non-vacuum deposition methods. The most common vacuum techniques that have been used to fabricate TiO_2 thin films for photocatalytic applications are atomic layer deposition [15] and sputtering methods [16]. Non-vacuum solution based methods, however, have several advantages compared to vacuum based techniques, such as cost-effectiveness, resource savings, and rapid deposition.

The most common non-vacuum technique that was used to fabricate TiO_2 thin films for photocatalytic applications is the sol–gel method (Supplementary Materials Table S1). Among them, many studies have been done on the gas-phase photocatalytic degradation of acetaldehyde [17–22] and acetone [22–27] on TiO_2 thin films, while a few studies were done on photocatalytic oxidation of MTBE and heptane. Supplementary Materials Table S1 shows that the photocatalytic decomposition of MTBE and heptane was mostly studied on TiO_2 powder coatings [27–31]. In our previous study, TiO_2 thin films were examined for photocatalytic conversion of gaseous MTBE on the TiO_2 surface. The TiO_2 film deposited on window glass exhibited conversion of MTBE of approximately 80% [5]. To the best of our knowledge, no prior studies have examined photodecomposition of heptane on transparent TiO_2 thin films. As seen in Supplementary Materials Table S1, the results of these studies are hardly comparable due to the different evaluation techniques and reactor types besides operating conditions during photocatalytic tests, such as pollutant type, flow rate, temperature, irradiation intensity, and photocatalytic coating area.

Among the non-vacuum solution based techniques, spray pyrolysis is a robust, cost-effective, and easily up-scalable chemical method [32,33]. In the spray pyrolysis method, aerosols are generated by a nebulizer (e.g., pneumatic, ultrasonic, or electrostatic) or an ultrasonic generator and carried in a gas flow through a furnace [34,35] or onto a hot plate [5]. Among the various nebulization techniques available, the use of ultrasonic spray pyrolysis (USP) was favoured because of the generation of small-sized initial droplets, and the inherent low velocity of the initially formed aerosol [35].

Despite the several advantages of USP-synthesized thin films, no publications on the decomposition of VOCs such as acetone, acetaldehyde, and heptane on transparent TiO_2 thin films fabricated by USP reporting their photocatalytic activity regarding the materials characteristics were found available; thus, this study supplies more insights into this topic. The present paper is a comprehensive study of TiO_2 thin films synthesized by USP and applied for the abatement of different VOCs.

Hereby, two purposes were considered for this study: firstly, to evaluate the photocatalytic performance of TiO_2 thin films deposited at different temperatures; and secondly, to investigate the effect of humidity, airflow regime, and light source (i.e., UV and VIS) on the abatement of air pollutants on TiO_2 thin films. MTBE, acetone, acetaldehyde, and heptane were individually used to evaluate the photocatalytic activity for gas-phase reactions in the multi-section plug-flow reactor.

2. Results

2.1. Material Characterization

2.1.1. Surface Morphology

Figure 1 shows the surface morphology of as-prepared TiO_2 thin films on borosilicate glass. TiO_2 film deposited at 350 °C (Figure 1a) showed a plane surface structure, whereas the film deposited at 450 °C (Figure 1c) showed a grain-like structure. The thickness of TiO_2 films sprayed at 350 and 450 °C were 190 and 330 nm (Table 1), respectively, as estimated from the cross-sectional scanning electronic microscope (SEM) images (inset in Figure 1a,c).

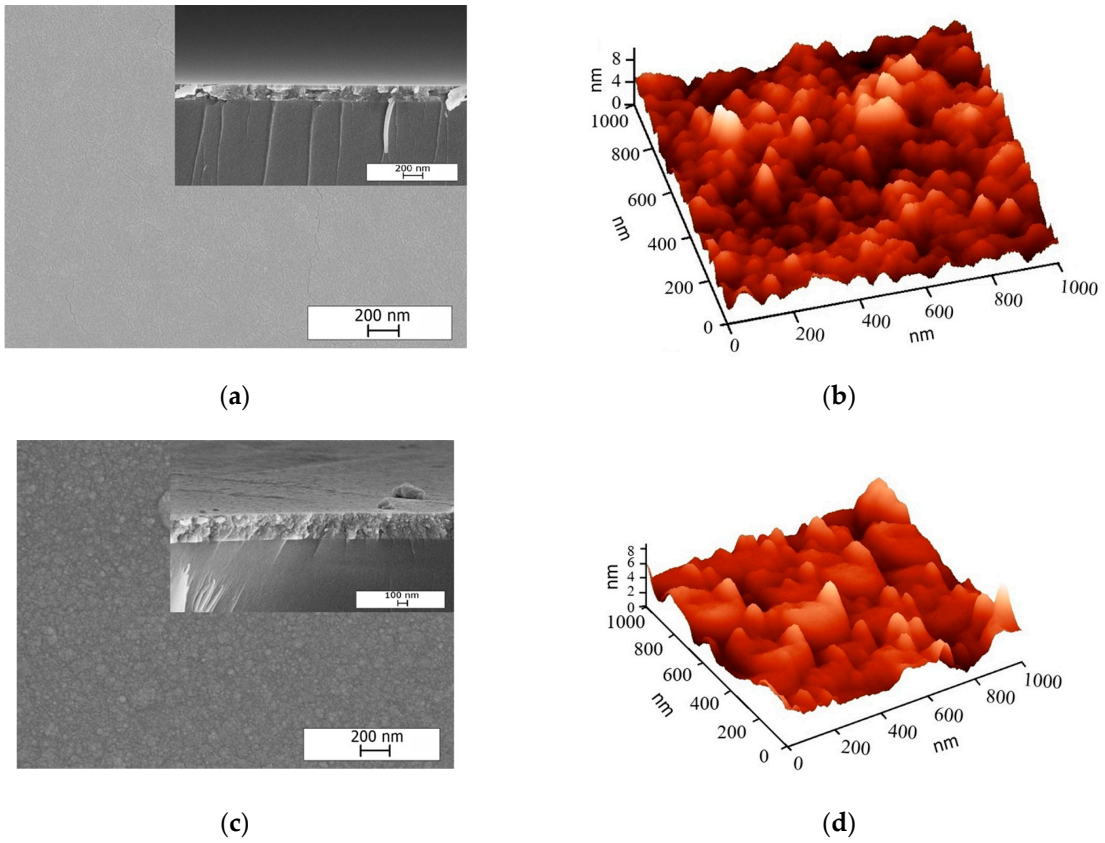

Figure 1. SEM surface image (**a**,**c**) and AFM image (**b**,**d**) of as-prepared TiO_2 thin films deposited on borosilicate glass at 350 and 450 °C. Insets of (**a**) and (**c**) show the cross-sectional SEM images of the corresponding TiO_2 thin films.

Table 1. XPS results. Summary of different ratios obtained by XPS data for the aged-TiO_2 thin films before and after UV-treatment.

Deposition Temperature (°C)	Aged-TiO_2 Samples (before UV-Treatment)		After UV-Treatment	
	(Vo)/(Ti–O) (at%/at%)	(OH^-)/(Ti–O) (at%/at%)	(Vo)/(Ti–O) (at%/at%)	(OH^-)/(Ti–O) (at%/at%)
350	0.17	0.08	0.12	0.11
450	0.09	0.30	0.09	0.05

Figure 1b,d depicts three-dimensional (3-D) atomic force microscope (AFM) images of TiO_2 films on borosilicate substrate. TiO_2 thin films deposited at 350 °C showed grains with a size of ca 50 nm. TiO_2 films deposited at 450 °C showed grains with a size of ca 50 nm and agglomerated grains with a

size of ca 200 nm. Different surface topography of the films deposited at 350 to 450 °C resulted also in a slight increase of the root mean square (RMS) roughness from 0.6 to 1.0 nm, respectively. The SEM and AFM images revealed the formation of agglomeration as elliptical clusters for the TiO_2 thin film deposited at 450 °C. The formation of agglomerated grains was observed in TiO_2 thin films deposited by spray pyrolysis at high temperatures [36].

2.1.2. Structural Properties

Figure 2 shows the XRD patterns of TiO_2 films deposited at 350 and 450 °C onto borosilicate glass. The XRD patterns exhibited reflection peaks at 2 theta of 25.3°, 37.9°, 48.1°, 54.1°, and 55.2° corresponding to reflections from (101), (004), (200), (105), and (211) crystal planes of the anatase structure (JCPDS 01-070-6826) [37]. No other crystalline phases of TiO_2 were detected. The Scherrer formula was applied to calculate the mean crystallite size of TiO_2 films using the (101) peak of the anatase phase. Similar mean crystallite sizes of 26 and 22 nm were found for the TiO_2 films deposited at 350 and 450 °C, respectively. This confirms that deposition temperature did not have any remarkable effect on the structural properties of sprayed TiO_2 thin films.

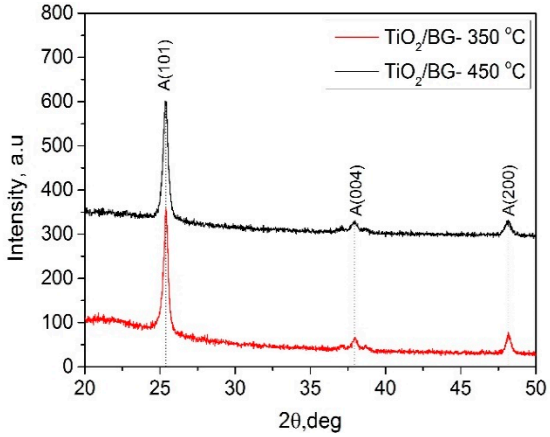

Figure 2. XRD patterns of TiO_2 films deposited at 350 and 450 °C onto borosilicate glass. All films were annealed at 500 °C for 1 h in air.

2.1.3. Optical Properties

Figure 3 shows the total transmittance spectra of TiO_2 thin films deposited at 350 and 450 °C and annealed at 500 °C for 1 h. Both TiO_2 films showed total transmittance of ca. 80% in the visible spectral region. The indirect band gap of the TiO_2 film was determined according to the Tauc plot [5]. The optical band gap of both samples was found to be 3.38 eV (inset of Figure 3).

2.1.4. XPS Study

XPS is a useful and sophisticated measurement technique for investigating the chemical constituents of a material, the ionic states of the constituent elements, and the ratio of the amounts of the different ionic states of a single constituent element. Estimation of oxygen vacancies and carbon species was confirmed from the XPS data in many studies [38–42] with the deconvoluted O1s and C1s XPS spectrum of the TiO_2.

The surface chemical composition and bonding structure of the aged and UV-treated TiO_2 thin films were investigated with the analysis of XPS data. Figures 4 and 5 show the O1s and C1s core level spectra of the surface of aged-TiO_2 thin films deposited at 350 and 450 °C before and after UV-treatment, respectively. The asymmetric O1s and C1s core level peaks were deconvoluted by using Lorentzian–Gaussian (function pseudo-Voigt) fitting analysis. The background subtraction was applied by using Shirley type fitting [5].

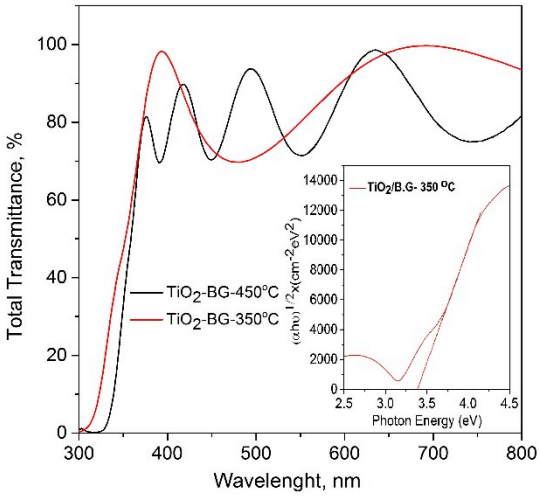

Figure 3. Total transmittance spectra of as-prepared TiO_2 thin films. The inset shows the optical band gap value of the TiO_2 thin film deposited at 350 °C.

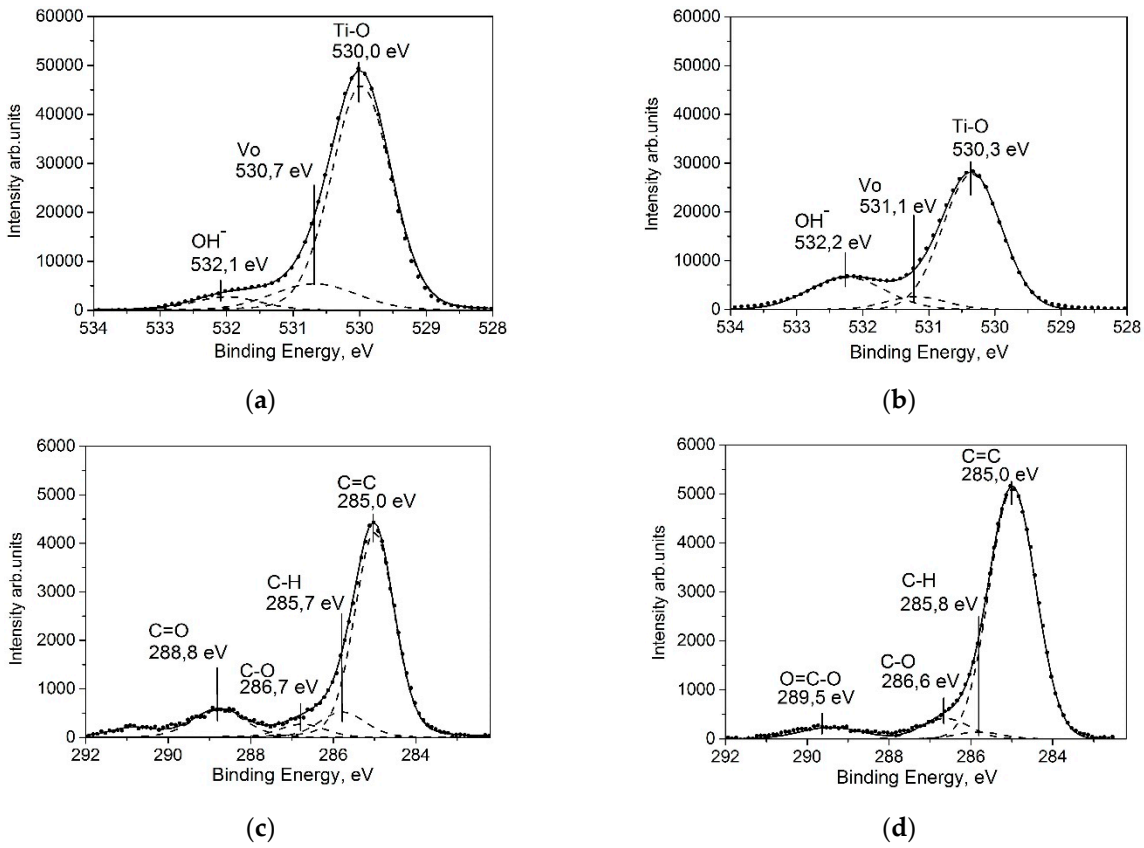

Figure 4. XPS spectra of aged-TiO_2 thin films deposited at (**a**) 350 and (**b**) 450 °C in the binding energy (BE) region of O1s. XPS spectra of aged-TiO_2 thin films deposited at (**c**) 350 and (**d**) 450 °C in the BE region of C1s.

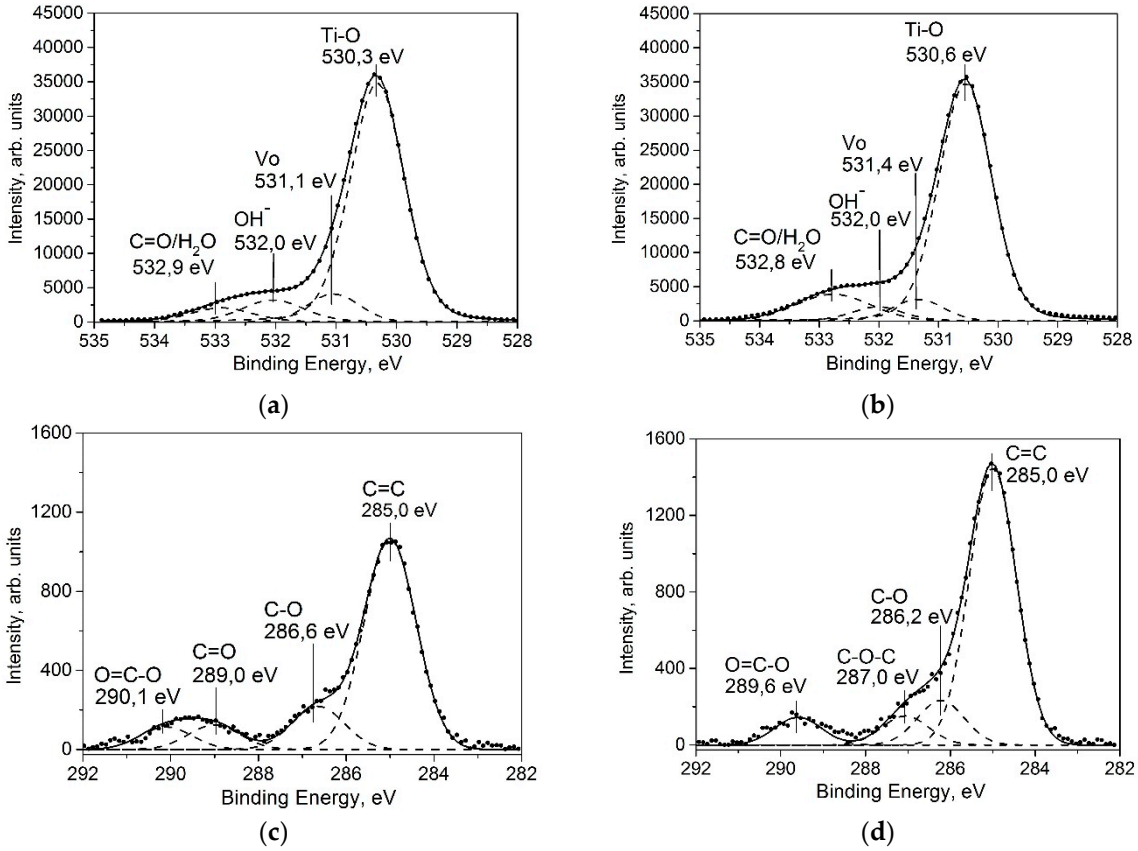

Figure 5. XPS spectra of aged-TiO_2 thin films after UV surface cleaning. TiO_2 thin films deposited at (**a**) 350 and (**b**) 450 °C in the BE region of O1s. XPS spectra of TiO_2 thin films deposited at (**c**) 350 and (**d**) 450 °C in the BE region of C1s.

XPS Data Analysis of Aged-TiO_2 Thin Films

The O1s core level peak of the aged-TiO_2 thin films was deconvoluted into three peaks (Figure 4a,b). The peak observed in binding energy (BE) value at 530.0 ± 0.3 eV was assigned to the Ti–O bond and the peak at BE value at 530.7 ± 0.4 eV was ascribed to the presence of oxygen vacancy defects (Vo). In addition, the peak at 532.1 ± 0.1 eV was attributed to surface hydroxyl groups (OH^-), revealing that the film surface contained adsorbed surface OH^- groups [43–45].

Figure 4c,d show the C1s core level spectra of aged-TiO_2 thin films deposited at 350 and 450 °C, respectively. The spectra could be resolved into four peaks at BE of 285.0, 285.7, and 286.7, ±0.1, and 288.8 ± 0.3 eV. In both TiO_2 samples, the C1s peaks located at 285.0 and 285.7 ± 0.1 eV corresponded to C=C and C–C/C–H, respectively [43]. It is highly probable that hydrocarbons and other carbon-like species could be formed on the surface of TiO_2 layers as a result of preparation procedure or due to carbon contamination arising from aging of samples in ambient atmosphere [43,46]. Further, there were other peaks observed at 286.7 ± 0.1, 288.8 (Figure 4c), and 289.6 eV (Figure 4d) that belonged to oxygen species containing carbonyl moieties, such as C–O, C=O, and O=C–O, respectively [41–43,47,48].Moreover, the peak positioned at 290.07 ± 0.4 eV could have resulted from the π–π shake-up process (Figure 4c) [42].

The Scofield' cross-sections were applied to investigate the integrated areas of O1s core level spectra for the calculation of atomic concentrations of the components, such as Ti–O, Vo, and OH^- presented in the O1s and C1s core level spectrums. The ratios of the components (OH)/(Ti–O) and (Vo)/(Ti–O) are shown in Table 1. As seen in Table 1, the amount of oxygen vacancies ((Vo)/(Ti–O) ratios) on the surface of TiO_2 films decreased from 0.17 up to 0.09 with the increase in the deposition temperature from 350 to 450 °C. This result agrees with our previous study, showing that the amount

of oxygen vacancies decreases with increasing deposition temperature [5]. The lower number of oxygen vacancy defects on TiO_2 thin films deposited at 450 °C can be attributed to the effect of the high heat deposition temperature that repairs the surface oxygen defects [5]. It should be noted that the deposition temperature has a large effect on the properties of TiO_2 films deposited by spray pyrolysis. Even though the TiO_2 thin films were exposed to annealing treatment at high temperatures, it was shown in our previous studies that the structural, morphological, and chemical properties of TiO_2 thin films were found to depend on the film deposition temperature [5,32,49]. As seen in Table 1, the aged-TiO_2 films showed an increase in the amount of OH^- groups on the film surface with increasing deposition temperature. In the literature, it was observed that there is an inconsistency trend on the amount of OH^- groups on the film surface concerning the increase in the film thickness [42] and heat treatment [48]. Simonsen et al. [48] reported that the surface of the TiO_2 films grown by microwave assisted sol–gel at 550 °C had the lowest amount of surface OH^- groups, while the hydroxyl groups on the film surface increased gradually with an increase in calcination temperature from 25 to 450 °C. A similar fluctuation in the amount of OH^- groups was observed also in our previous study [5].

XPS Data Analysis of Aged-TiO_2 Thin Films after UV-Treatment

Figure 5 represents the O1s and C1s core level spectra of UV-treated aged-TiO_2 thin films fabricated at 350 and 450 °C.

The O1s core level spectra of the surface of the UV-treated aged-TiO_2 thin films could be deconvoluted into four peaks (Figure 5a,b). The peaks at 530.3 ± 0.3, 531.1 ± 0.3, and 532.0 eV were assigned as Ti–O, Vo, and OH^-, respectively. In the literature, the peak observed in the BE value at 532.9 ± 0.1 was associated with different species, such as C–O, C=O, or chemisorbed-H_2O molecules [41,50]. As seen in Table 1, after UV-treatment, the TiO_2 thin film deposited at 350 °C possessed a higher level of oxygen vacancies on the top of the film surface compared to the 450 °C deposited sample. The amount of hydroxyl groups ((OH)/(Ti–O), Table 1), however, decreased considerably after UV treatment in the case of the TiO_2 thin film sprayed at 450 °C.

A smaller amount of carbon species was observed on the surface of TiO_2 thin films after UV-treatment (Figure 5c,d) compared to XPS results of aged-TiO_2 films (Figure 4c,d), showing the modification of the surface composition of aged-TiO_2 films after UV-treatment. Similar to the aged-TiO_2 samples, the peaks at the BE values of 285.0 and 286.6 ± 0.4 and 289.6 ± 0.5 eV were attributed to C=C, C–O, and O=C–O, respectively [45–48]. The peak at 287.0 eV in the carbon spectra of the TiO_2 sample grown at 450 °C (Figure 5d) could be assigned as C–O–C [45]. In the case of the TiO_2 film grown at 350 °C, the peak at BE value at 289.0 eV (Figure 5) could be assigned to C=O [41,45]. In addition, it should be noted that the peak located in BE energy at 285.7 attributed to C–H (Figure 4c,d) was not observed in C1s spectra of the UV-treated TiO_2 thin films (Figure 5c,d) due to the decomposition of hydrocarbons on the top of the TiO_2 film surface by the UV treatment [41,51].

2.2. Wettability

The water contact angles (WCA) for as-prepared TiO_2 films deposited at 350 and 450 °C were 12 and 17°, respectively. The films were aged in air over a month, and the increase was observed up to 46 and 55° (Figure 6). The increase in the WCA during aging could be due to the formation of a hydrocarbon layer on the film surface in air (Table 1) [52].

As seen in Figure 6, short UV irradiation of 5 min decreased the WCA of TiO_2 film deposited at 350 °C from 46.8° to 10°. Further UV irradiation (in total 10 min) decreased the WCA even up to 0°. Thus, this revealed that a relatively short UV irradiation time of 5 min was necessary to modify the surface behavior of TiO_2 film deposited at 350 °C from hydrophilic to superhydrophilic. Opposite to that, the WCA of TiO_2 films deposited at 450 °C decreased gradually from 55° to 0° within 35 min (Figure 6).

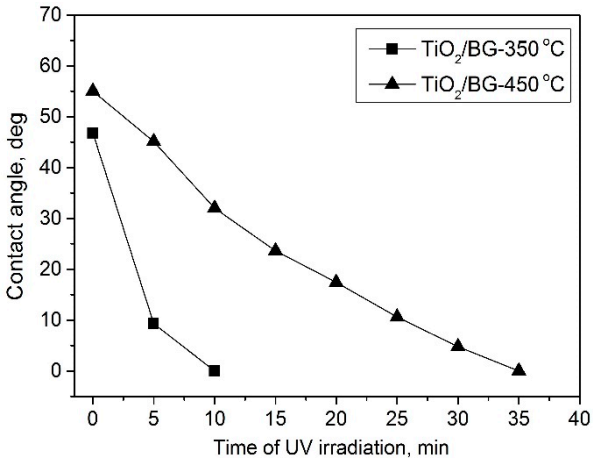

Figure 6. Plot of the WCA of the aged TiO_2 films deposited at 350 and 450 °C vs time of UV irradiation.

Different behaviors of WCA under UV-irradiation of TiO_2 films deposited at 350 and 450 °C can be explained by different surface chemical compositions of TiO_2 thin films. The changes in the degree of hydroxyl groups, oxygen defects, and hydrocarbons present on the TiO_2 surface could be related to the rapid wettability conversion (in total 10 min) of the TiO_2 thin film deposited at 350 °C, correlated with the results obtained by XPS.

In comparison to TiO_2 films, the amount of hydroxyl groups was found to be considerably higher in the TiO_2 thin film deposited at 350 °C after UV irradiation (Table 1), compared to films deposited at 450 °C. This can be explained by the high amount of inherent oxygen vacancy defects on the surface of aged-TiO_2 films (Table 1), leading to the trapping of hydroxyl groups that enhanced the hydrophilic surface [41,42,53]. Moreover, the rapid wetting ability of the TiO_2 sample deposited at 350 °C could be due to the difference in the ability of photodecomposition of the hydrocarbon layer on the TiO_2 surface [51,54].

2.3. Photocatalytic Activity

2.3.1. The Effect of Deposition Temperature on Photocatalytic Activity of TiO_2 Thin Films

Figure 7 shows the photocatalytic conversion of MTBE (10 ppm) on TiO_2 thin films deposited at 350 and 450 °C. Operating conditions for the experimental runs were: residence time 15.6 s per section, relative humidity (RH) 6%, and reactor temperature 34 °C.

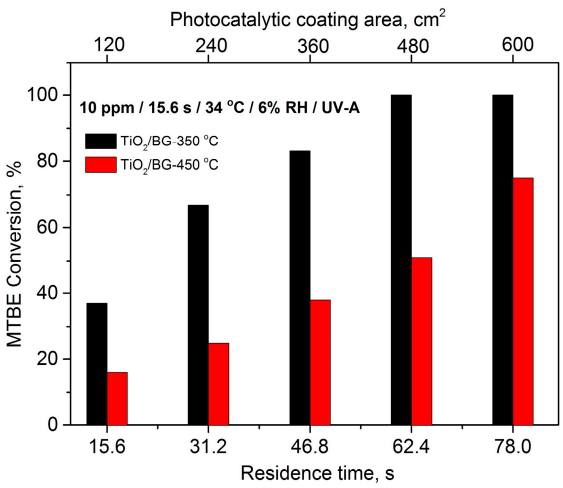

Figure 7. Photocatalytic conversion of MTBE on as-prepared TiO_2 thin films deposited onto glass substrates at 350 and 450 °C; MTBE inlet concentration 10 ppm; RH 6%.

As seen in Figure 7, the TiO_2 thin films deposited at 350 °C showed higher photocatalytic activity than TiO_2 thin films deposited at 450 °C. The MTBE at the initial concentration of ca.10 ppm was completely converted to CO_2 and H_2O at a residence time of 62.4 s on the TiO_2 thin films deposited at 350 °C, while TiO_2 thin films deposited at 450 °C exhibited MTBE conversion of ca. 75% after 78 s. The higher photocatalytic activity of TiO_2 thin film deposited at 350 °C can be ascribed to several factors including the surface morphology, higher level of oxygen vacancy defects, and OH^- groups on the film surface compared to the samples deposited at 450 °C (Table 1). It is a well-known phenomenon that the presence of the surface-active OH^- groups benefit photocatalytic reactions. It was reported that OH^- groups can participate directly in the interface reactions by trapping photo-generated holes that diffuse to TiO_2 surfaces and producing reactive surface hydroxyl radicals. They can also act as active sites for adsorption/reaction of reactant molecules on TiO_2 [55]. Further, there is a mutual effect between the photo-induced electrons bound by oxygen vacancies and the adsorbed O_2, and thus oxygen vacancies can support O_2 adsorbing [56]. This indicates that oxygen vacancies can favor the adsorbed O_2 to capture photo-induced electrons, simultaneously producing reactive oxygen species (ROS) and, thus, promoting the oxidation of organic substances. Therefore, it can be suggested that oxygen vacancies and other surface defects are in favor of photocatalytic reactions [57].

In the present study, the formation of large grains was observed on the TiO_2 thin film deposited at 450 °C compared to that of the films deposited at 350 °C (Figure 1a,c) due to the agglomeration of grains during the deposition process at higher temperature. This could be one additional reason for the reduction of the photocatalytic activity of TiO_2 films deposited at 450 °C. It was reported that the surface area decreases with the increase in the grain size, which is unfavorable for the enhancement of photocatalytic efficiency [58,59]. Furthermore, the agglomeration decreases the interface between the grains, and thus leads to the reduction of surface active sites available for photocatalytic reactions [59,60].

Further study of the characterization of gas-phase photocatalytic activity of synthesized thin films was carried out with the TiO_2 films deposited at 350 °C due to their higher photocatalytic activity ascertained with MTBE.

2.3.2. The Effect of Air Humidity on Photocatalytic Activity of TiO_2 Thin Films

VOCs, such as MTBE, acetone, acetaldehyde, and heptane were chosen as single model air pollutants for this study. The effect of different operating conditions, i.e., humidity, inlet concentration of pollutant, residence time, and source of irradiation, on the photocatalytic process performance was studied. The effect of increase in air humidity from ca. 6 to 40% RH on photocatalytic oxidation of heptane, acetaldehyde, acetone, and MTBE is presented in Figure 8 (residence time in reactor section was 15.6 s).

The results showed that under lower humidity the conversions of heptane, acetaldehyde, and acetone were 46, 74, and 93% at residence time of 78 s, respectively, and 100% conversion of MTBE was achieved at 62.4 s, as previously discussed (Figure 8a). During the photocatalytic oxidation of those VOCs, tert-butyl formate (TBF) and formic acid were detected as intermediate gas-phase products of MTBE and heptane, respectively. Under a relatively dry atmosphere, the formation of intermediate products followed by their degradation was observed. There was an increase in the concentration of formic acid achieving its maximum at residence time of 46.8 s and subsequently it decreased with the further increase in residence time (at 78.0 s, 1% of degraded heptane emerged as gaseous formic acid), whereas no TBF was observed at residence time of 78 s as this intermediate product was completely degraded.

Air humidity usually dually affects the photodegradation processes. It can contribute to surface re-hydration of photocatalysts, which could lead to the increase in concentration of •OH radicals and hence to an increase in reaction rate. Competitive adsorption between water vapor and the organic compounds, which inhibits the binding of reactant molecules, is also common at higher water vapor content in reactors [61]. Therefore, the effect of air humidity on the performance of photocatalytic

oxidation of MTBE, acetone acetaldehyde, and heptane were investigated on TiO_2 thin films deposited at 350 °C. As could be observed from Figure 8a,b, the conversion efficiency of most VOCs diminished with the increase in the relative humidity from 6 to 40%.

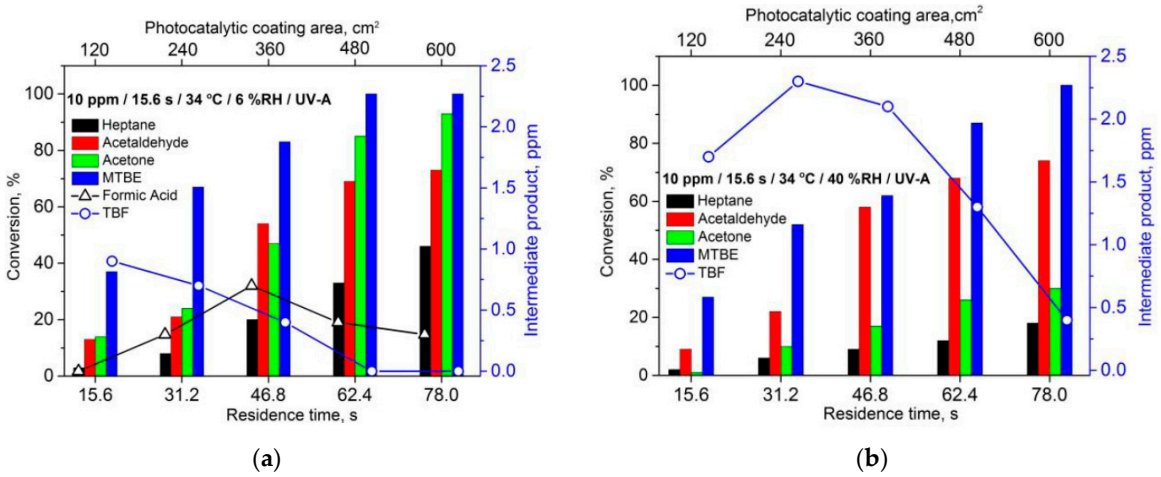

Figure 8. Photocatalytic conversion of different VOCs on TiO_2 thin film deposited at 350 °C under (**a**) dry (6% RH) air and (**b**) humid (40% RH) air conditions. VOCs inlet concentration 10 ppm.

The conversion of heptane decreased almost twice with the increase in the relative humidity. In contrast to dry air, in humid air no gaseous organic intermediate products of heptane were monitored, as formic acid was expected to stay adsorbed on the surface of hydrated photocatalyst film.

Humid atmosphere influenced also the formation of the MTBE intermediate product TBF and retarded slightly the overall degradation of MTBE. Complete conversion of MTBE on a coated glass with the surface area of TiO_2 thin film deposited at 350 °C of 600 cm^2 (78 s) was achieved also under humid air conditions. Only TBF was found as an intermediate product from the degradation of MTBE in dry and humid conditions. In dry air, TBF was converted to CO_2 and H_2O at a residence time of 62.4 s, while the detected amount of TBF was higher at a higher humidity (at 78.0 s, 5% of degraded MTBE appeared as gaseous TBF). Thus, the increase in air humidity was slightly hindering the photocatalytic mineralization of MTBE on thin films.

Acetone degradation was affected by relative humidity, showing a sharp drop in the conversion of acetone from 93 to 30%. No gas-phase intermediate products were detected in either dry or humid air during photodegradation of acetone over TiO_2 films. It is interesting to note that acetone is a polar molecule, which is supposed to penetrate through water to the surface of TiO_2. However, in the present study, it was seen that higher humidity (40% RH) showed a detrimental effect on the adsorption and photocatalytic decomposition of acetone. Similar results were observed during the photodecomposition of acetone [28] and chlorobenzene [62], which are soluble in water, on the TiO_2 surface under high humidity conditions.

The only compound of which oxidation was uninfluenced by variations in air humidity was acetaldehyde. There were no significant changes in the conversion of acetaldehyde (approx. 75% conversion at 78 s) with the increase in relative humidity from 6 to 40%. No gas-phase products other than CO_2 and H_2O were observed during the photocatalytic degradation of acetaldehyde in both dry and humid air conditions (Figure 8a,b). It is known that transport of the reactant molecules through water molecules depends on the solubility of the molecules of interest in water. Acetaldehyde is a polar molecule, which is water-soluble. This explains the "immunity" of photocatalytic oxidation of acetaldehyde molecules to the difference in air humidity. Generalizing, it could be assumed that the potential influence of air humidity on the performance of thin films depends not only on the character of the initial compounds to be oxidized, but also on the character (adsorption affinity, ease of degradation) of the intermediate products. The difference in the trend of acetone and acetaldehyde degradation

under humid conditions is assumed to be attributed to the formation of intermediate products, which in case of acetone presumably deteriorate the overall performance of the photocatalytic process.

2.3.3. The Effect of Residence Time and Inlet Concentration of VOCs on Photocatalytic Activity of TiO_2 Thin Films

The effect of shorter residence time and lower inlet concentration of VOCs was examined on the surface of TiO_2 thin film with initial pollutant concentration of 5 ppm and relative decrease in residence time in the reactor section from 15.6 to 7.8 s (Figure 9).

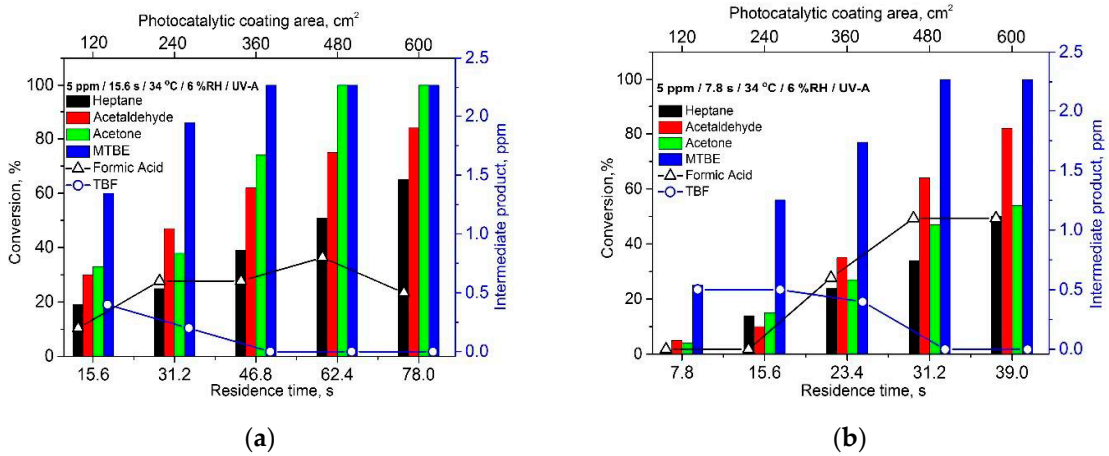

Figure 9. Photocatalytic conversion of different VOCs on TiO_2 thin film deposited at 350 °C under different airflow rates (**a**) 0.5 L min^{-1} (15.6 s per section) and (**b**) 1.0 L min^{-1} (7.8 s per section) VOC inlet concentration 5 ppm; RH 6%.

The decrease in inlet concentration of VOCs from 10 to 5 ppm (Figures 8a and 9a) resulted in higher conversions of all model compounds. With the decrease in concentration from 10 to 5 ppm in 78 s the conversion of heptane increased from 46 to 65% (4.6 and 3.3 ppm of heptane degraded, respectively) and conversion of acetaldehyde increased from 74 to 85% (7.4 and 4.2 ppm of acetaldehyde degraded, respectively), whereas complete degradation of 5 ppm of acetone and MTBE was obtained within ca. 62 and 47 s, respectively, while 93% of acetone with initial concentration of 10 ppm was degraded (9.3 ppm) in 78 s. Thus, despite the lower conversions of VOCs at higher initial concentrations, the increase in inlet concentration leads to the larger absolute amounts of the degraded compounds.

The residence time in the reactor section shifted from 15.6 to 7.8 s with the increase in the airflow rate from 0.5 L min^{-1} to 1.0 L min^{-1}. Generally, when the airflow rate is increased, two opposing processes can be envisaged: the decrement in residence time and the enhancement in mass transfer rate, which are, respectively, inhibiting and promoting factors in photocatalytic oxidation processes [63]. By reducing the residence time, the pollutants a have shorter time for adsorption on the surface and participating in oxidation reactions. As seen in Figure 9b, a general decrease in the conversion of VOCs was observed within five sections of the reactor, i.e., on the same photocatalytic surface area (600 cm^2), but with a twice shorter residence time if compared to the results in Figure 9b. If comparing the same residence time in the reactor at different airflow regimes, then at shorter residence time of 15.6 s (one section of reactor in Figure 9a and two sections in Figure 9b) there is a decrease in the conversions of VOCs despite the higher photocatalytic area in two sections of the reactor in Figure 9b. However, at residence time of 31.2 s (two sections of the reactor in Figure 9a and four sections in Figure 9b), the two times higher airflow rate is favoring the photocatalytic oxidation of VOCs at higher photocatalytic surface: the conversions of all the compounds increased from 25, 38, 47, and 86% to 34, 47, 64, and 100% for heptane, acetone, acetaldehyde, and MTBE, respectively. The process of photocatalytic oxidation of acetaldehyde and MTBE was revealed as especially benefitting from the intensification of mass transfer

in the reactor at the same residence time. Thus, again, the effect of the different airflow regimes was expected to be different for each VOC.

The order in conversion of VOCs at residence time of 39 s in five sections was MTBE > acetaldehyde > acetone > heptane (Figure 9b), while it was MTBE > acetone > acetaldehyde > heptane at longer residence time (Figure 9a). For instance, the conversion of acetaldehyde and MTBE was affected slightly by shorter residence time, while the impact of shorter residence time was remarkable for photocatalytic decomposition of acetone. A sharp decrease in the conversion of acetone from 100% at residence time of 62.4 s (Figure 9a) to 47% at residence time of 31.2 s (Figure 9b) was observed on the same photocatalytic surface area of 480 cm^2 (four sections), whereas high conversions of acetaldehyde (82% conversion at 39.0 s) and MTBE (100% conversion at 31.2 s) were easily achievable at shorter residence time (Figure 9b). This could be attributed to the different reaction rates of each VOCs. Ibrahim et al. [64] studied the kinetics model of degradation of acetone and acetaldehyde on Degussa P25. It was reported that initial reaction rate of acetaldehyde exceeded that of acetone by more than six times (833 and 125 μmol m^{-3} min^{-1}, respectively).

2.3.4. The Effect of Irradiation Source on Photocatalytic Activity of TiO_2 Thin Films

The photocatalytic activity of TiO_2 thin films sprayed at 350 °C was evaluated with 5 ppm MTBE and acetone in gas-phase under visible light in dry air (Figure 10). TiO_2 thin film showed MTBE conversion of 60% and acetone conversion of 33% at residence time of 78 s. Under the same operating conditions except light source (UV-A light), the sample showed 100% conversion of MTBE at residence 46.8 (360 cm^2) and 100% conversion of acetone at residence time 62.4 s (480 cm^2) (Figure 9a). The remarkable reduction in photocatalytic activity of TiO_2 film was due to the optical gap width of stoichiometric TiO_2 (>3.1 eV) determining its photocatalytic activity under the action of near UV radiation, which constitutes only a small percent of the visible light spectrum [65,66].

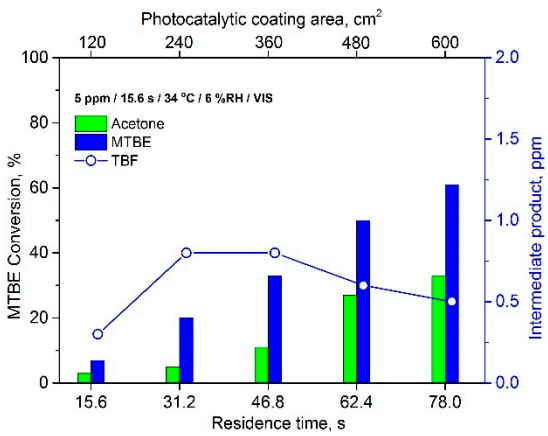

Figure 10. Photocatalytic conversion of MTBE and acetone on TiO_2 thin film deposited at 350 °C under visible light. MTBE and acetone inlet concentration 5 ppm; RH 6%; residence time 15.6 s per section.

TBF was detected as gaseous intermediate of MTBE, while no gaseous intermediate products were monitored during the decomposition of acetone. The highest amount of TBF was observed at residence time of 46.8 s, which was 0.8 ppm of TBF from 1.65 ppm of degraded MTBE (48% of MTBE transformed to TBF). At higher residence times, the amount of TBF on TiO_2 thin film was steadily decreasing, achieving 16% of degraded MTBE oxidized to TBF at 78 sec. In comparison, the TiO_2 thin film was capable of overcoming by-product accumulation at a surface area residence time of 46.8 s (360 cm^2) under UV-A light (Figure 9a); moreover, under UV-A light with the same other parameters, no other gaseous products than water and carbon dioxide were observed.

The visible-light-activity of TiO_2 could be related to the defect disorder and the consequent electronic structure. Firstly, it could be ascribed to the formation of oxygen defects on the film surface

(Table 1). It was proposed that the oxygen vacancy defects act as shallow trapping sites, which is related to the formation of some sub-bands in the electronic band structure of TiO_2, considered as the main dominating factor of the visible emission [32]. Additionally, it was observed that TiO_2 thin films still have oxidized carbon species after UV irradiation (C–O, C=O, O=C–O, etc.) on the surface of TiO_2 film, (Figure 5a), known as defect-containing sp^2-hybridized carbons. It was reported that these defect-associated functional groups (carbon species) provide surface active sites, which influence the effective charge transfer [47–67].

3. Materials and Methods

3.1. Thin Film Synthesis and Materials Characterization

TiO_2 thin films were fabricated by USP onto borosilicate glass at 350 and 450 °C. The TiO_2 thin films were annealed at 500 °C for 1 h in air in a furnace and are labelled as as-prepared samples throughout the article. The details of the solution preparation and the operating parameters of ultrasonic spray pyrolysis were reported in our previous study [5]. Borosilicate glass was selected as a substrate for TiO_2 thin films since it contains few Na^+ ions, unlike soda-lime glass substrates [68]; it is known that Na^+ ions have a detrimental effect on photocatalytic activity [68].

Zeiss HR FESEM Ultra 55 SEM (Jena, Germany) with an acceleration voltage of 4.0 kV was performed to obtained surface morphology and the film thickness. NT-MDT Solver 47 PRO AFM system was used to study the surface morphology of the films. The AFM measurement was carried out in the non-contact mode (resolution in the range of 3 nm) and the samples were studied in 1 μm × 1 μm area per scans. The RMS roughness analysis was performed through the 3-D AFM scan according to the ISO 4287/1 standards.

X-ray diffraction (XRD) measurements were performed with a Rigaku Ultima IV diffractometer (Tokyo, Japan) with CuKα radiation (ʎ = 1.5406 A°, 40 kV at 40 mA). The thin films were studied in grazing-incidence diffraction geometry using PBA (parallel beam analyzer 0.112 deg.) soller slit. The angle between the film surface and the incident beam was fixed at 0.5°. The scintillation detector was used during the measurements. The measurements were carried out in 2 theta configurations with the 2 theta range of 20–50°, with a step of 0.02°. The MCS of thin films was calculated by the Scherrer method using the FWHM (full width at half maximum) of the (101) reflection of the TiO_2 anatase phase.

The total transmittance spectra of the TiO_2 films on borosilicate glass were measured in the wavelength range of 300–800 nm on a Jasco V-670 UV–VIS–NIR spectrophotometer equipped with a 40 nm integrating sphere.

XPS studies were performed on a Kratos Axis Ultra DLD (delayline detector) spectrometer in conjunction with a 165 mm hemispherical electron energy analyzer. The analysis was carried out with monochromatic Al Kα X-rays (1486.6 eV) operating at 15 kV and 225 W. All XPS spectra were recorded using an aperture slot of 300–700 mm and pass energy of 20 eV. The spectra were calibrated using C1s core level peak centered data at a binding energy of 285.0 eV. XPS measurements were carried out for the aged-TiO_2 thin films before and after UV treatment. UV treatment was applied for 12 hours to the aged-TiO_2 thin films in ambient air with an Actinic BL 15 W fluorescent lamp for removing contaminants from the TiO_2 thin film surface.

Wettability of the films was determined by water contact angle (WCA) measurements. DSA 25 (KRUSS Instrument) was carried out at room temperature. A sessile drop fitting method was applied for WCA measurements. Actinic BL 15 W fluorescent lamp (Philips), with max emission at 365 nm, was used to investigate the dependence of WCA of aged-TiO_2 films on UV irradiation under ambient conditions.

3.2. Photocatalytic Measurements

The photocatalytic activity of TiO_2 thin films was studied in a five-section plug-flow photocatalytic reactor with a section volume of 130 mL. Details of the reactor setup were reported in a previous

study [5]. MTBE ($C_2H_{12}O$), acetone (C_3H_6O), acetaldehyde (C_2H_4O), and heptane (C_7H_{16}) were used as model air pollutants (all reagents ≥ 99% purity). The inlet concentrations of the gaseous pollutant were 5 and 10 ppm. The relative humidity was maintained at 6 ± 1% and 40 ± 5% for dry and humid air conditions, respectively. In the photocatalytic experimental setup, air flows of 0.5 and 1 L min^{-1} were used, which gave the residence time of 15.6 or 7.8 s per reactor section, respectively. The temperature in the reactor was not additionally regulated; equilibrium was reached between the surrounding temperature, heating by the UV-A lamps, and application of reflectors resulting in 33 ± 2 °C. The following lamps such as UV Philips Actinic BL 15 W with an average irradiance of 3.5 mW cm^{-2} with reflector (integrated in the range of 180–400 nm, with max emission at 365 nm, UV-B/UV-A ratio < 0.2%), or VIS Philips TL-D 15 W, irradiance 3.3 mW cm^{-2} with reflector (integrated in the range of 180–700 nm, UV/UV VIS ratio < 5%) were used as the UV and VIS sources. Irradiance from UV and VIS sources was measured by a fiber optic spectrometer (USB-2000 + UV–VIS, Ocean Optics).

MTBE, acetone, acetaldehyde, and heptane peaks were quantified by INTERSPEC 200-X FTIR spectrometer with a Specac Tornado 8-m gas cell at the IR bands of 1063–1124, 1172–1245, 2630–2910, and 2825–3010 cm^{-1}, respectively. The gas-phase intermediate products of MTBE and heptane, TBF and formic acid, respectively, were also quantitatively monitored by means of FTIR at the IR bands from 1138 to 1190 and from 1103 to 1107 cm^{-1}, respectively.

4. Conclusions

TiO_2 thin films were deposited by ultrasonic spray pyrolysis on borosilicate glass substrates at 350 and 450 °C, followed by annealing at 500 °C for 1 h in air. Photocatalytic activity of TiO_2 thin films were evaluated as a function of their morphological, structural, and optical properties. According to the SEM cross-sectional images, the thickness of TiO_2 films deposited at 350 and 450 °C were 190 and 330 nm, respectively. TiO_2 films possess smooth surface morphology, showing the RMS roughness in the range of 0.6–1 nm. The films consist of an anatase crystalline structure with the mean crystallite size in the range of 22–26 nm and indicate total transmittance of 80% in the visible spectral region. XPS study confirmed that UV-treatment was effective to reduce the amount of hydrocarbons on the film surface and to modify the surface chemical composition. It was confirmed that after UV-treatment, the surface of TiO_2 films deposited at 350 °C possessed higher amounts of oxygen vacancy defects and hydroxyl groups ((Vo)/(Ti–O) = 0.12, (OH)/(Ti–O) = 0.11) compared to the films deposited at 450 °C ((Vo)/(Ti–O) = 0.09, (OH)/(Ti–O) = 0.05). The rapid photoinduced hydrophilic to superhydrophilic conversion of TiO_2 thin film deposited at 350 °C revealed the importance of the high-level oxygen vacancy defects, related to the enhancement of hydroxyl groups on the film surface.

Photocatalytic activity tests of TiO_2 thin films revealed that the films deposited at 350 °C with surface area of 480 cm^2 effectually degraded 100% of the MTBE, whereas TiO_2 thin film deposited at 450 °C showed the MTBE conversion of ca. 75% with a surface area of 600 cm^2. TiO_2 thin film deposited at 350 °C with surface area of 600 cm^2 effectually degraded, 90% of acetone and 75% of acetaldehyde vapor (inlet 10 ppm) under dry air (6% RH) conditions without the formation of gas-phase intermediate products. Complete degradation of MTBE as well as 80% conversion of acetaldehyde were also achieved under humid air (40% RH) conditions at residence time of 78 s. With the decrease in inlet concentration from 10 to 5 ppm the increase in conversion efficiency of heptane and acetaldehyde was obtained at residence time of 78 s, whereas complete degradation of 5 ppm of acetone and MTBE was obtained within ca. 62 and 47 s, respectively. TiO_2 thin films deposited at 350 °C were photocatalytically active under visible light degrading 60% of MTBE and 33% of acetone (inlet 5 ppm).

Based on the conducted analysis, it could be concluded that the amount of oxygen vacancy and hydroxyl groups on the TiO_2 surface highly influences the photocatalytic activity and wettability of sprayed TiO_2 thin films. This study demonstrated that TiO_2 thin films prepared by ultrasonic spray pyrolysis are sufficient to degrade different VOCs under different air conditions and irradiation sources and thereby are prospective coatings for self-cleaning and air purification applications.

Supplementary Materials: The following are available online at http://www.mdpi.com/2073-4344/9/11/915/s1, Table S1: Literature overview on photocatalytic decomposition of acetaldehyde acetone MTBE, and heptane on different TiO_2 thin films prepared by non-vacuum methods.

Author Contributions: I.D. carried out the thin film deposition and material characterizations (XRD, optical properties, and wettability test), attended data collection for the photocatalytic activity test, took part in the design of the all figures and tables, participated in the writing of the manuscript, and drafted the manuscript. M.K. (Marina Krichevskaya) carried out the photocatalytic activity test and interpretation of data, and participated in the writing of the manuscript. A.K. made the XPS data analysis. I.O.A. carried out the design of the study, participated in data analysis, and was associated with preparing of the manuscript. M.K. (Malle Krunks) participated in data analysis. All authors gave final approval for publication.

Funding: I.D. is supported by the Estonian Ministry of Education and Research, Estonian Research Council project IUT19-4, Estonian Centre of Excellence project TK141 and EU regional Fund project 2014-2020.4.01.16-0032. I.O.A., M.K. (Malle Krunks), and A.K. are supported by the Estonian Ministry of Education and Research, Estonian Research Council projects IUT19-4 and Estonian Centre of Excellence project TK141. M.K. (Marina Krichevskaya) is supported by the Estonian Ministry of Education and Research, Estonian Research Council projects IUT1-7. This work was partially supported by ASTRA 'TUT Institutional Development Programme for 2016–2022' Graduate School of Functional Materials and Technologies (2014-2020.4.01.16-0032).

Acknowledgments: The authors acknowledge V. Mikli for SEM, M. Danilson for XPS measurements, and A. O. Titilope for AFM measurements.

Conflicts of Interest: The authors declare no conflict of interest.

References

1. Wallace, L.A. *The Total Exposure Assessment Methodology (TEAM) Study Summary and Analysis*; U.S. Environmental Protection Agency: Washington, DC, USA, 1987; pp. 59–73.
2. Schmidt, M.C.; Buchbinder, A.M.; Weitz, E.; Geiger, M.F. Photochemistry of the indoor air pollutant acetone on Degussa P25 TiO_2 studied by chemical ionization mass spectrometry. *J. Phys. Chem. A* **2007**, *111*, 13023–13031. [CrossRef]
3. Chang, C.P.; Chen, J.N.; Lu, M.C. Heterogeneous photocatalytic oxidation of acetone for air purification by near UV-irradiated titanium dioxide. *J. Environ. Sci. Health A* **2003**, *38*, 1131–1143. [CrossRef]
4. FarLend, W.H.; United States Environmental Protection Agency. *Health and Environmental Effects Document for N-Heptane: Final Draft*; EPA: Washington, DC, USA, 1989; p. 5.
5. Dundar, I.; Krichevskaya, M.; Katerski, A.; Oja Acik, I. TiO_2 thin films by ultrasonic spray pyrolysis as photocatalytic material for air purification. *R. Soc. Open Sci.* **2019**, *6*, 181578. [CrossRef]
6. Schiewecka, A.; Uhdea, E.; Salthammera, T.; Salthammer, L.C.; Morawska, L.; Mazaheric, M.; Kumar, P. Smart homes and the control of indoor air quality. *Renew. Sustain. Energy Rev.* **2018**, *94*, 705–718. [CrossRef]
7. Degallaix, M.C. Air cleaning devices: A growing market polluted by confusing communication-certified performances for air cleaners. *J. Rehva* **2017**, *1*, 49–51.
8. Mamaghani, A.H.; Haghighat, F.; Lee, C.S. Photocatalytic oxidation technology for indoor environment air purification: The state-of-the-art. *Appl. Catal. B Environ.* **2017**, *203*, 247–269. [CrossRef]
9. Alonso-Telleza, A.; Massona, R.; Robert, D.; Kellera, N.; Keller, V. Comparison of Hombikat UV100 and P25 TiO_2 performance in gas-phase photocatalytic oxidation reactions. *J. Photochem. Photobiol. A Chem.* **2012**, *250*, 58–65. [CrossRef]
10. Bianchia, C.L.; Gatto, S.; Pirola, C.; Naldoni, A.; Michele Di, A.; Cerrato, G.; Crocellàd, V.; Capucci, V. Photocatalytic degradation of acetone, acetaldehyde and toluene in gas-phase: Comparison between nano and micro-sized TiO_2. *Appl. Catal. B Environ.* **2014**, *146*, 123–130. [CrossRef]
11. Šuligoja, A.; Urška Lavrenčič Štangara, U.L.; Ristić, A.; Mazaj, M.; Verhovšekc, D.; Tušar, N.N. TiO_2–SiO_2 films from organic-free colloidal TiO_2 anatase nanoparticles as photocatalyst for removal of volatile organic compounds from indoor air. *Appl. Catal. B Environ.* **2016**, *184*, 119–131. [CrossRef]
12. Shayegan, Z.; Lee, C.S.; Haghighat, F. TiO_2 photocatalyst for removal of volatile organic compounds in gas phase—A review. *Chem. Eng. J.* **2018**, *334*, 2408–2439. [CrossRef]
13. Verbruggen, S.W.; Deng, S.; Kurttepeli, M.; Cott, D.J.; Vereecken, P.M.; Bals, S.; Detavernier, C.; Lenaerts, S. Photocatalytic acetaldehyde oxidation in air using spacious TiO_2 films prepared by atomic layer deposition on supported carbonaceous sacrificial templates. *Appl. Catal. B Environ.* **2014**, *160–161*, 204–210. [CrossRef]

14. Arabatzis, I.M.; Antonaraki, S.; Stergiopoulos, T.; Hiskia, A.; Papaconstantinou, E.; Bernard, M.C.; Falaras, P. Preparation, characterization and photocatalytic activity of nanocrystalline thin film TiO_2 catalysts towards 3,5-dichlorophenol degradation. *J. Photochem. Photobiol. A* **2012**, *149*, 237–245. [CrossRef]
15. Buchalska, M.; Surowka, M.; Hamalainen, J.; Livonen, T.; Leskela, M.; Macyk, W. Photocatalytic activity of TiO_2 films on Si support prepared by atomic layer deposition. *Catal. Today* **2015**, *252*, 14–19. [CrossRef]
16. Stefanov, B.I.; Niklasson, G.A.; Granqvist, C.G.; Österlund, L. Gas-phase photocatalytic activity of sputter-deposited anatase TiO_2 films: Effect of 001 preferential orientation, surface temperature and humidity. *J. Catal.* **2016**, *335*, 187–196. [CrossRef]
17. Tryba, B.; Jafari, S.; Sillanpää, M.; Nitta, A.; Ohtanic, B.; Morawski, A.W. Influence of TiO_2 structure on its photocatalytic activity towards acetaldehyde decomposition. *Appl. Surf. Sci.* **2019**, *470*, 376–385. [CrossRef]
18. Seo, H.O.; Woo, T.G.; Park, E.J.; Cha, B.J.; Kim, I.H.; Wook, H.S.; Kim, Y.D. Enhanced photocatalytic activity of TiO_2 films by removal of surface carbon impurities; the role of water vapor. *Appl. Surf. Sci.* **2017**, *420*, 808–816. [CrossRef]
19. Blount, C.M.; Kim, D.H.; Falconer, J.L. Transparent thin-film TiO_2 photocatalysts with high activity. *Environ. Sci. Technol.* **2001**, *35*, 2988–2994. [CrossRef]
20. Negishi, N.; Matsuzawa, S.; Takeuchi, K.; Pichat, P. Transparent Micrometer-Thick TiO_2 films on SiO_2-coated glass prepared by repeated dip-coating/calcination: Characteristics and photocatalytic activities for removing acetaldehyde or toluene in air. *Chem. Mater.* **2007**, *19*, 3808–3814. [CrossRef]
21. Watanabe, T.; Fukayama, S.; Masahiro, M.; Fujishima, A.; Hashimoto, K. Photocatalytic activity and photo-induced wettability conversion of TiO_2 thin film prepared by sol-gel process on a soda-lime glass. *J. Sol-Gel Sci. Technol.* **2000**, *19*, 71–76. [CrossRef]
22. Yao, N.; Yeung, K.L. Investigation of the performance of TiO_2 photocatalytic coatings. *Chem. Eng. J.* **2011**, *167*, 13–21. [CrossRef]
23. Kluson, P.; Luskova, H.; Cajthaml, T.; Solcova, O. Non thermal preparation of photoactive titanium (IV) oxide thin layers. *Thin Solid Films* **2006**, *495*, 18–23. [CrossRef]
24. Yu, J.C.; Yu, J.; Zhao, J. Enhanced photocatalytic activity of mesoporous and ordinary TiO_2 thin films by sulfuric acid treatment. *Appl. Catal. B Environ.* **2002**, *36*, 31–43. [CrossRef]
25. Yu, C.J.; Yu, J.; Ho, W.; Zhao, J. Light-induced super-hydrophilicity and photocatalytic activity of mesoporous TiO_2 thin films. *J. Photochem. Photobiol. A Chem.* **2002**, *148*, 331–339. [CrossRef]
26. Coronado, J.M.; Zorn, M.E.; Tejedor-Tejedor, I.; Anderson, M.A. Photocatalytic oxidation of ketones in the gas phase over TiO_2 thin films: A kinetic study on the influence of water vapor. *Appl. Catal. B Environ.* **2003**, *43*, 329–344. [CrossRef]
27. Maudhuit, A.; Raillard, C.; Héquet, V.; Le Coq, L.; Sablayrolles, J.; Molins, L. Adsorption phenomena in photocatalytic reactions: The case of toluene, acetone and heptane. *Chem. Eng. J.* **2011**, *170*, 464–470. [CrossRef]
28. Shang, J.; Du, Y.; Xu, Z. Photocatalytic oxidation of heptane in the gas-phase over TiO_2. *Chemosphere* **2002**, *46*, 93–99. [CrossRef]
29. Galanos, E.; Poulopoulos, S.; Philippopoulos, C. Photocatalytic destruction of methyl tert butyl ether in the gas phase using titanium dioxide. *J. Environ. Sci. Health A* **2002**, *9*, 1665–1675. [CrossRef]
30. Park, W.E.; Joo, H.; Kang, J.W. Photodegradation of methyl tertiary butyl ether vapor with immobilized titanium dioxide. *Sol. Energy Mater. Sol. Cells* **2003**, *80*, 73–84. [CrossRef]
31. Preis, S.; Kachina, A.; Santiago, C.N.; Kallas, J. The dependence on temperature of gas-phase photocatalytic oxidation of methyl tert-butyl ether and tert-butyl alcohol. *Catal. Today* **2005**, *101*, 353–358. [CrossRef]
32. Oja Acik, I.; Mere, A.; Krunks, M.; Solterbeck, C.H.; Es-Souini, M. Properties of TiO_2 films prepared by the spray pyrolysis method. In *Solid State Phenomena*; Trans Tech Publications: Baech, Switzerland, 2004; Volume 99, pp. 259–264. [CrossRef]
33. Polivtseva, S.; Oja Acik, I.; Katerski, A.; Mere, A.; Mikli, V.; Krunks, M. Spray Pyrolysis deposition of Sn_xS_y thin films. *Energy Procedia* **2014**, *60*, 156–165. [CrossRef]
34. Perednis, D.; Gauckler, L.J. Thin film deposition using spray pyrolysis. *J. Electroceram.* **2005**, *14*, 103–111. [CrossRef]
35. Bang, J.H.; Didenko, Y.; Helmich, R.J.; Suslick, K.S. Nanostructured materials through ultrasonic spray pyrolysis. *Mater. Matters* **2012**, *7*, 15–20.

36. Raut, N.C.; Mathews, T.; Chandramohan, P.; Srinivasan, M.P.; Dash, S.; Tyagi, A.K. Effect of temperature on the growth of TiO2 thin films synthesized by spray pyrolysis: Structural, compositional and optical properties. *Mater. Res. Bull.* **2011**, *46*, 2057–2063. [CrossRef]
37. Powder Diffraction File (PDF), (PDF-2/Release 2013 RDB) (01-070-6826) (archived on 1 November 2019).
38. Dupin, J.; Gonbeau, D.; Vinatier, P.; Levasseur, A. Systematic XPS studies of metal oxides, hydroxides and peroxide. *Phys. Chem. Chem. Phys.* **2000**, *2*, 1319–1324. [CrossRef]
39. Bharti, B.; Kumar, S.; Lee, H.; Kumar, R. Formation of oxygen vacancies and Ti^{3+} state in TiO_2 thin film and enhanced optical properties by air plasma treatment. *Nat. Sci. Rep.* **2016**, *6*, 32355. [CrossRef]
40. Sarkar, A.; Khan, G. The formation and detection techniques of oxygen vacancies in titanium oxide-based nanostructures. *Nanoscale* **2019**, *11*, 3414–3444. [CrossRef]
41. Huang, Y.; Tien, H.; Ma, C.; Yang, S.; Wu, S.; Liu, H.; Mai, Y. Effect of extended polymer chains on properties of transparent graphene nanosheets conductive film. *J. Mater. Chem.* **2011**, *21*, 18236–18241. [CrossRef]
42. Amor, S.; Jacquet, M.; Fioux, P.; Nardin, M. XPS characterization of plasma treated and zinc oxide coated PET. *Appl. Surf. Sci.* **2009**, *255*, 5052–5061. [CrossRef]
43. Gromyko, I.; Krunks, M.; Dedova, T.; Katerski, A.; Klauson, D.; Oja Acik, I. Surface properties of sprayed and electrodeposited ZnO rod layers. *Appl. Surf. Sci.* **2017**, *405*, 521–528. [CrossRef]
44. Chen, W.; Koshy, P.; Christopher, S.C. Effects of film topology and contamination as a function of thickness on the photo-induced hydrophilicity of transparent TiO_2 thin films deposited on glass substrates by spin coating. *J. Mater. Sci.* **2016**, *51*, 2465–2480. [CrossRef]
45. Jimmy, C.; Yu, J.; Yuk, T.H.; Zhang, L. Effect of surface microstructure on the photoinduced hydrophilicity of porous TiO_2 thin films. *J. Mater. Chem.* **2002**, *12*, 81–85. [CrossRef]
46. McCafferty, E.; Wightman, J.P. Determination of the concentration of surface hydroxyl groups on metal oxide films by a quantitative XPS method. *Surf. Interface Anal.* **1998**, *26*, 549–564. [CrossRef]
47. Li, J.; Tang, S.; Lu, L.; Zeng, H.C. Preparation of nanocomposites of metals, metal oxides, and carbon nanotubes via self-assembly. *J. Am. Chem. Soc.* **2007**, *129*, 9401–9409. [CrossRef] [PubMed]
48. Zhang, L.; Zhang, J.; Jiu, H.; Ni, C.; Zhang, X.; Xu, M. Graphene-based hollow TiO_2 composites with enhanced photocatalytic activity for removal of pollutants. *J. Phys. Chem. Solids* **2015**, *86*, 82–89. [CrossRef]
49. Oja, I.; Mere, A.; Krunks, M.; Nisumaa, R.; Solterbeck, C.; Es-Souni, M. Structural and electrical characterization of TiO_2 films grown by spray pyrolysis. *Thin Solid Films* **2006**, *515*, 674–677. [CrossRef]
50. Simonsen, M.E.; Li, Z.; Søgaard, E.G. Influence of the OH^- groups on the photocatalytic activity and photoinduced hydrophilicity of microwave assisted sol–gel TiO_2 film. *Appl. Surf. Sci.* **2009**, *255*, 8054–8062. [CrossRef]
51. Ohtsu, N.; Masahashi, N.; Mizukoshi, Y.; Wagatsuma, K. Hydrocarbon decomposition on a hydrophilic TiO_2 surface by UV-irradiation: Spectral and quantitative analysis using in-situ XPS technique. *Langmuir* **2009**, *25*, 11586–11591. [CrossRef]
52. Holtzinger, C.; Rapenne, L.; Chaudouet, P.; Berthome, G.; Langlet, M. Thickness effects in naturally superhydrophilic TiO_2–SiO_2 nanocomposite films deposited via a multilayer sol–gel route. *J. Sol-Gel Sci. Technol.* **2012**, *64*, 465–479. [CrossRef]
53. Simonsen, M.E.; Sørensen, M.B.; Søgaard, E.G. Comparison of methods for evaluation of activity of photocatalytic films. *Environ. Sci. Pollut. Res.* **2012**, *19*, 3772–3781. [CrossRef]
54. Zheng, J.; Bao, S.; Guo, Y.; Jin, P. Natural hydrophobicity and reversible wettability conversion of flat anatase TiO_2 thin film. *ACS Appl. Mater. Interfaces* **2014**, *63*, 1351–1355. [CrossRef]
55. Chen, H.; Nanayakkara, E.C.; Grassian, V. Titanium dioxide photocatalysis in atmospheric chemistry. *Chem. Rev.* **2012**, *112*, 5919–5948. [CrossRef] [PubMed]
56. Sakai, N.; Fujishima, A.; Watanabe, T.; Hashimoto, K. Quantitative evaluation of the photoinduced hydrophilic conversion properties of TiO_2 thin film surfaces by the reciprocal of contact angle. *J. Phys. Chem. B* **2003**, *107*, 1028–1035. [CrossRef]
57. Jing, L.Q.; Qu, Y.C.; Wang, B.Q.; Li, S.D.; Jiang, B.J.; Yang, L.B.; Fu, W.; Fu, H.G.; Sun, J.Z. Review of photoluminescence performance of nano-sized semiconductor materials and its relationships with photocatalytic activity. *Sol. Energy Mater. Sol. Cells* **2006**, *90*, 1773–1787. [CrossRef]
58. Akbarzadeh, R.; Umbarkar, B.S.; Sonawane, S.R.; Takle, S.; Dongare, K.M. Vanadia–titania thin films for photocatalytic degradation of formaldehyde in sunlight. *Appl. Catal. A* **2010**, *374*, 103–109. [CrossRef]
59. Li, X.; Yu, J.; Jaroniec, M. Hierarchical photocatalysts. *Chem. Soc. Rev.* **2016**, *45*, 2603–2636. [CrossRef]

60. Rehman, S.; Ullah, R.; Butt, A.M.; Gohar, N.D. Strategies of making TiO_2 and ZnO visible light active. *J. Hazard. Mater.* **2009**, *170*, 560–569. [CrossRef]
61. Neti, N.R.; Parmar, G.R.; Bakardjieva, S.; Subrt, J. Thick film titania on glass supports for vapour phase photocatalytic degradation of toluene, acetone, and ethanol. *Chem. Eng. J.* **2010**, *163*, 219–229. [CrossRef]
62. Demeestere, K.; Dewulf, J.; Van Langenhove, H.; Sercu, B. Gas–solid adsorption of selected volatile organic compounds on titanium dioxide Degussa P25. *Chem. Eng. Sci.* **2003**, *58*, 2255–2267. [CrossRef]
63. Mamaghani, A.H.; Haghighat, F.; Lee, C. Photocatalytic degradation of VOCs on various commercial titanium dioxides: Impact of operating parameters on removal efficiency and by products generation. *Build. Environ.* **2018**, *138*, 275–282. [CrossRef]
64. Ibrahim, H.; de Lasa, H. Kinetic Modeling of the Photocatalytic Degradation of Air-Borne Pollutants. *AIChE J.* **2004**, *50*, 1017–1027. [CrossRef]
65. Pelaez, M.; Nolan, N.T.; Pillai, S.C.; Seery, M.K.; Falaras, P.; Kontos, A.G.; Dunlop, P.S.M.; Hamilton, J.W.; Byrne, J.A.; O'Sheaf, K.; et al. A review on the visible light active titanium dioxide photocatalysts for environmental applications. *Appl. Catal. B Environ.* **2012**, *125*, 331–349. [CrossRef]
66. Valeeva, A.A.; Kozlova, E.A.; Vokhmintsev, A.S.; Kamalov, R.V.; Dorosheva, I.B.; Saraev, A.A.; Weinstein, I.A.; Rempel, A.A. Nonstoichiometric titanium dioxide nanotubes with enhanced catalytical activity under visible light. *Sci. Rep.* **2018**, *8*, 9607. [CrossRef] [PubMed]
67. Yu, J.; Maa, T.; Liu, S. Enhanced photocatalytic activity of mesoporous TiO_2 aggregates by embedding carbon nanotubes as electron-transfer channel. *Phys. Chem. Chem. Phys.* **2011**, *13*, 3491–3501. [CrossRef] [PubMed]
68. Krysa, J.; Novotna, P.; Kment, S.; Mills, A. Effect of glass substrate and deposition technique on the properties of sol-gel TiO_2 thin films. *J. Photochem. Photobiol. A* **2011**, *222*, 81–86. [CrossRef]